Cement and Concrete Composites 95 (2019) 81–91

Contents lists available at ScienceDirect

Cement and Concrete Composites

journal homepage: www.elsevier.com/locate/cemconcomp

Effect of gypsum content in sprayed cementitious matrices: Early age hydration and mechanical properties

C. Herrera-Mesen[a,*], R.P. Salvador[b], S.H.P. Cavalaro[c,**], A. Aguado[a]

[a] Department of Civil and Environmental Engineering, Barcelona Tech, Polytechnic University of Catalonia, UPC, Jordi Girona 1-3, 08034, Barcelona, Spain
[b] Department of Civil Engineering, São Judas Tadeu University, 546 Taquari St., 03166-000, São Paulo, Brazil
[c] School of Architecture, Building and Civil Engineering, Loughborough University, Leicestershire, LE11 3TU, UK

ARTICLE INFO

Keywords:
Sprayed materials
Sulfate balance
Accelerators
Hydration
Mechanical strength

ABSTRACT

Sprayed materials must present short setting times and a fast early strength development for safety and productivity reasons. In order to improve these characteristics, the construction industry has focused on the development of new formulations of accelerators. Research and improvement of other components of the mix, such as cement or additions, have not advanced at the same rate despite being also crucial for the reaction kinetics. The objective of this work is to evaluate the influence of gypsum content on the hydration and mechanical strength development in sprayed mixes. Sprayed pastes and mortars were prepared with one type of cement, two types of accelerators and different gypsum contents. Kinetics, mechanisms of hydration and mechanical properties were evaluated. Results showed a better performance in sprayed mixes that contain ideal doses of gypsum. Such approach provides valuable information for the improvement of the formulation of cement used in sprayed concrete applications.

1. Introduction

Sprayed cementitious materials are widely used in the construction industry, from buildings to infrastructure. In some of these applications, accelerators are added to achieve faster setting, to reduce rebound and to improve initial strength, adhesiveness and cohesiveness of the sprayed cementitious materials [1,2]. Accelerators incorporate dissolved aluminate ions into the matrix, thus modifying the kinetics and mechanisms of hydration of cement [3–5]. These ions react with the sulfates from cement to form calcium sulfoaluminate hydrates, which promote an early development of mechanical properties [6].

The molar aluminate-to-sulfate ratio (C_3A/SO_3) is a key parameter that regulates the accelerator reaction. Ettringite is the main hydrate formed if the C_3A/SO_3 ratio is between 0.67 and 0.90 [6]. This is hardly ever the case in accelerated matrices since the additional amount of aluminate ions provided by accelerators generally leads to an undersulfated condition, characterized by C_3A/SO_3 ratios higher than 0.90. In this context, sulfates deplete rapidly, ettringite starts to be consumed by C_3A hydration and converts into monosulfoaluminate [7,8]. The early formed monosulfoaluminate covers cement particles and fills up the space available in the matrix. This decreases the rate and extent of alite hydration, producing lower compressive strengths at later ages [6] [9].

To mitigate such effect, the construction industry developed new formulations of alkali-free accelerators, which contain sulfate ions in their composition to balance the C_3A/SO_3 ratio. However, mixes with these accelerators may still behave as undersulfated [3,6,10] so that extra doses of sulfate are required to control C_3A and C_4AF hydration. A proper addition of gypsum to the cement or the composition of the matrix may provide a valid and inexpensive extra source of sulfates to change the C_3A/SO_3 ratio towards an optimum compatibility with the accelerators.

Little attention has been paid to the improvement of the composition of the matrix, whereas efforts have focused on the improvement of the accelerator formulation. Consequently, there is still space left for improving the matrix-accelerator compatibility by defining better matrices. This study explores such approach and assesses its validity. The main objective here is to evaluate the influence of the gypsum content on the hydration behaviour and on the mechanical strength development in sprayed mixes containing accelerators.

An experimental program was conducted with sprayed pastes and

* Corresponding author.
** Corresponding author.
E-mail addresses: carlos.herrera.mesen@estudiant.upc.edu (C. Herrera-Mesen), S.Cavalaro@lboro.ac.uk (S.H.P. Cavalaro).

https://doi.org/10.1016/j.cemconcomp.2018.10.015
Received 16 May 2018; Received in revised form 18 October 2018; Accepted 22 October 2018
Available online 24 October 2018
0958-9465/

mortars produced with one type of cement, two types of accelerator and three different sulfate contents. Powder X-ray diffraction (XRD), isothermal calorimetry and scanning electron microscopy (SEM) were performed to evaluate the kinetics and mechanisms of hydration. Needle and pin penetration resistance and compressive strength were measured to evaluate the evolution of mechanical properties. To complete the analysis, water accessible porosity (WAP) was also determined in sprayed mortars.

All tests were performed with sprayed mixes because the mixing process of accelerated matrices significantly influences the reactivity of accelerators and the morphology of the hydrates formed [10]. Results obtained to provide a better understanding of how the sulfate balance in sprayed matrices influences their hydration and mechanical properties. Furthermore, they provide useful criteria for the design of cement and matrices specific for spraying, aiming to improve the compatibility with the accelerator.

2. Experimental program

Fig. 1 presents the diagram of the experimental program conducted in this study. Tests were performed with sprayed pastes and mortars at the Laboratorio de Estructuras Luis Agulló at the Polytechnic University of Catalonia (UPC) and at the Scientific and Technological Center from the University of Barcelona (CCIT-UB). The spraying procedure was based on recent publications by Galobardes et al. [1,11] in sprayed materials and by Salvador et al. [6,10] in sprayed pastes and mortars.

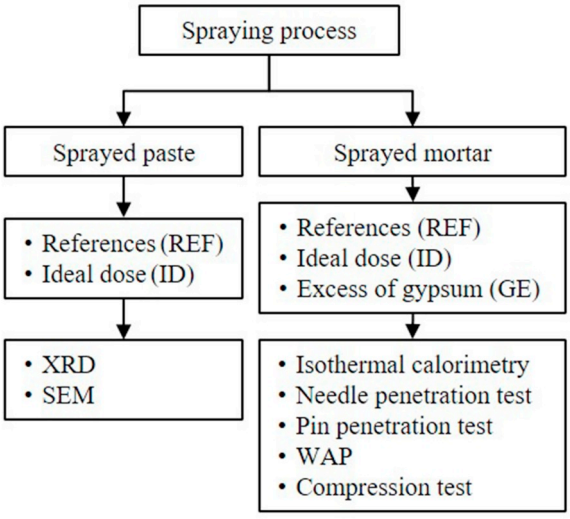

Fig. 1. Diagram of the experimental program conducted in the study.

2.1. Materials

An ordinary Portland cement type I (CEM I 52.5R) was used in this study. Table 1 presents its chemical composition and phase composition determined by XRF spectrometry and XRD-Rietveld refinement, respectively. Its total sulfate ion (SO_4^{2-}) content was 4.23% by weight and it was determined by dissolving 1.00 g of cement in 10.00 g of concentrated HNO_3 (65%), according to [14]. The resulting solution was diluted in a 250 mL volumetric flask using deionized water (Mili-Q, 18 ohm) and analyzed by ion chromatography.

Table 1
Cement composition and specific surface.

Chemical composition		Mineralogical composition	
Oxide	Content (%)	Phase	Content (%)
CaO	62.6	C_3S	58.3
SiO_2	19.9	C_2S	11.2
Al_2O_3	4.7	C_4AF	13.4
SO_3	3.5	C_3A_c	4.1
Fe_2O_3	3.3	C_3A_o	0.6
MgO	1.9	CaO	1.1
K_2O	1.0	$Ca(OH)_2$	1.7
TiO_2	0.2	$CaCO_3$	1.9
Na_2O	0.1	$CaSO_4.2H_2O$	2.1
P_2O_5	0.1	$CaSO_4.0.5H_2O$	4.4
MnO	0.0	K_2SO_4	0.0
LOI	2.9	$K_2Ca(SO_4)_2{\cdot}H_2O$	1.1
		MgO	0.0
		$MgCO_3$	0.0
		Total	99.9
Specific Surface BET (m^2/g)	2.96		

In addition to Table 1, the particle size distribution of the cement (determined by laser diffraction) is shown in Fig. 2.

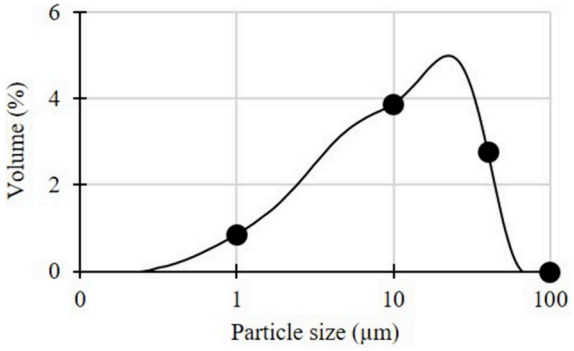

Fig. 2. Particle size distribution.

Distilled water and the Sikaplast® T1120 superplasticizer based on a polycarboxylate solution (34% of solid content) were also employed. In field conditions, the superplasticizer promotes the workability and pumpability of the mix. The same superplasticizer was employed in Refs. [1,3,10] for laboratory tests with sprayed matrices.

A limestone aggregate with a density of 2.32 g/cm^3 and with an absorption of 5.46% was used in the mortars. To avoid blockages of the spraying equipment, the particle size distribution of the aggregate ranged from 0 mm to 1.25 mm.

Table 2 shows the chemical composition of the alkali-free accelerator (AF) and the alkaline accelerator (AR) evaluated in this study. Both accelerators correspond to formulations commonly found in underground constructions.

Table 2
Chemical composition of accelerators.

Characteristics (mmol/g_{cement})	AF	AR
Solid content (%)	47.6	43.0
Dosage (% bcw)	5.0	3.0
Al_2O_3 (%)	13.5	24.0
SO_4^{2-} (%)	21.0	–
Na_2O (%)	–	19.0
pH at 20 °C	3.0	12.0
Al_2O_3/SO_4^{2-} molar ratio	0.6	–
Al_2O_3/Na_2O molar ratio	–	1.3

2.2. Mix composition

The composition of the mixes selected was based in recent publications [1,3,10,11]. In pastes, a water/cement (w/c) ratio of 0.32 was adopted. The superplasticizer dosage was 1.0% by cement weight (% bcw), according to the recommendation of the supplier. The AF accelerator was added at 5.0% bcw and the AR accelerator at 3.0% bcw. Both dosages were determined according to the procedure described in Ref. [1] to assure equivalent mechanical performance in pastes.

Mortars contained the same accelerators dosages as cement pastes. They had a sand/cement ratio of 1.7 by weight, w/c ratio equal to 0.51 and also contained superplasticizer at the dosage of 1.0% bcw. This composition presented an adequate workability for pumping and spraying (spread diameter equal to 300 mm with no bleeding, measured according to [12]). Although different w/c ratios were used for pastes and mortars, the tendencies in the chemical and mechanical behaviour observed are equivalent, because results are evaluated in a comparative manner depending on the gypsum content.

In pastes and mortars, additional gypsum was included to evaluate the influence of different sulfate contents on the chemical and mechanical performance of the matrix. Three different mixes were produced for each accelerator. Reference mixes (REF) contained only the sulfate of the cement (no additional gypsum was added). The ideal dose of gypsum (ID) corresponds to the amount of sulfate necessary to react with all the aluminate ions from the accelerators to form ettringite (Al/SO_4^{2-} equal to 0.66), without consuming gypsum from the cement. This ratio in the mixture is calculated according to equation (1).

$$\frac{Al_{(accelerator)}}{SO_4^{2-}{}_{(accelerator)} + SO_4^{2-}{}_{(accelerator)}} = 0.66 \quad (1)$$

The excess of gypsum (GE) corresponds to the additional amount of sulfate necessary to obtain ettringite as the final product from the reaction of the aluminate ions from the accelerator and from C_3A hydration. The amount of gypsum necessary to fulfil that requirement was calculated using equation (2).

$$\frac{Al_{(accelerator)} + Al_{(C3A)}}{SO_4^{2-}{}_{(cement)} + SO_4^{2-}{}_{(accelerator)} + SO_4^{2-}{}_{additional\ gypsum}} = 0.66 \quad (2)$$

In pastes, gypsum was incorporated as an addition to the other components, in order to maintain the same water/clinker and accelerator/clinker ratios. In mortars, gypsum replaced the corresponding amount of the aggregate, to maintain the same solid/liquid ratio of the matrix, according to equation (3).

$$\frac{Aggregate\ +\ Additional\ Gypsum}{Cement} = 1.7 \quad (3)$$

Table 3 presents the composition and nomenclature of each mix used in this study. The total gypsum content in the matrix corresponds to the sum of gypsum from cement and the additional gypsum used.

2.3. Mixing procedure

Pastes and mortars were prepared in a planetary mixer type 65/2 K-3 in single batches of approximately 40 L per case studied (see Table 3). This amount of material was needed to comply with the requirements of the spraying equipment, to assure a homogeneous flow of matrix through the pumping system and to fill up the panels for the tests [10,13].

In pastes, the cement and 90% of the total amount of water were mixed for approximately 2 min. The remaining 10% and the superplasticizer were pre-homogenized and the solution obtained was added and mixed for 2 min more. Then, the additional gypsum was added if applicable and all mixes were mixed for an additional 4 min. After that, pastes were kept at 20 °C until the spraying with the accelerators, which took place 1 h after the beginning of the mixing process.

The delayed incorporation of accelerators was already adopted by Refs. [10,13] to reproduce the conditions found in applications of sprayed matrices. Notice that, in practice, matrices commonly have to be transported to the worksite prior to being sprayed with accelerators. This procedure also contributes to a clearer assessment of the heat flow attributed to the accelerator reaction, which otherwise would overlap with the heat released during the initial mixing of cement and water.

The production of mortars followed the same steps as for the pastes. The only difference was the incorporation of the aggregates that took place at the moment of gypsum addition for ID and GE mixes. After that, mortars were kept at 20 °C until accelerator addition in order to follow the same procedure as in cement pastes. Finally, mortars were sprayed with accelerators 1 h after the beginning of mixing.

Table 3
Composition and nomenclature of mixes.

Accelerator	Additional gypsum (% by cement weight)	Total gypsum (% by clinker weight)	Nomenclature pastes	Nomenclature mortars
Alkali-free	–	7.58	PAF_REF	MAF_REF
	1.54	9.12	PAFG(ID)	MAFG(ID)
	7.42	15.00	–	MAFG(GE)
Alkaline	–	7.58	PAR_REF	MAR_REF
	3.64	11.22	PARG(ID)	MARG(ID)
	11.96	19.54	–	MARG(GE)

2.4. Spraying process

The wet-mix spraying process was used here since it is the most commonly employed to spray concrete around the world [11]. Fig. 3 presents the equipment, which corresponds to a small-scale version of a concrete spraying system used in previous research [10]. The whole spraying process was performed inside a climatic chamber at the temperature of 20 °C and relative humidity of 90%.

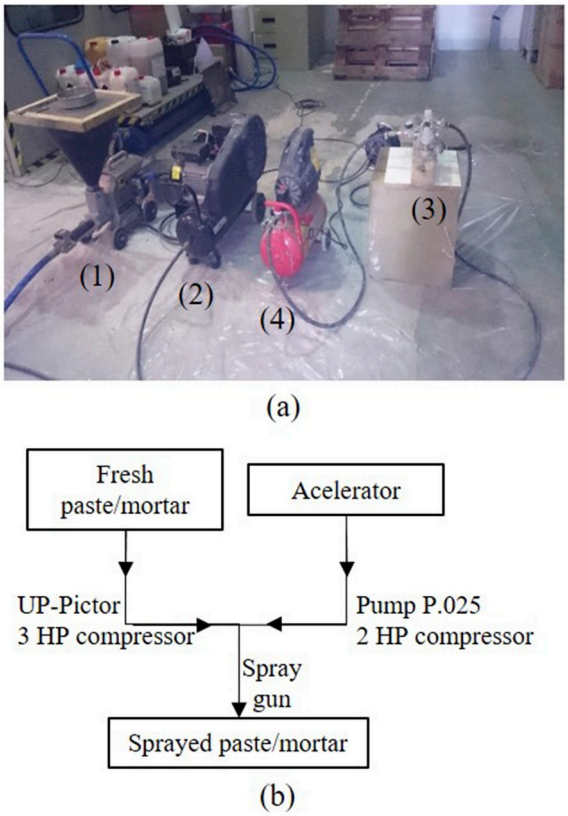

Fig. 3. (a) Spraying equipment in laboratory conditions and (b) diagram of the process.

The mix was pumped by the helical pump UP-Pictor (item #1, Fig. 3a), connected to the 3 HP-air compressor (item #2, Fig. 3a) and transported through the hose up to a spray gun. This type of pump is adequate for fluids like cement pastes and mortars in contrast with piston pumps that are indicated to handle fluids with coarser particles [14]. It also assures a more constant flow of material, eliminating the pulsation effect.

Accelerators were added at the spray gun by an air-operated diaphragm pump type P.025 (item #3, Fig. 3a) connected to a 2 HP-air compressor (item #4, Fig. 3a). This type of pump presented a homogeneous suction for all accelerators, although their viscosity varied according to their chemical composition.

Fig. 4 a shows in detail the spray gun of the equipment. The mix enters by the main pipe (item #1, Fig. 4a). Compressed air and accelerator entered by the inlets indicated by items #2 and #3 in Fig. 4 a, respectively. After that, they reached a chamber (item #5, Fig. 4a) where both components were mixed. Finally, accelerators and compressed air were homogenized with the cementitious matrix inside the nozzle (item #6, Fig. 4a) and the resulting mix was sprayed into the square, metallic panels. Fig. 4 b shows the panels, whose dimensions and distribution inside the climatic chamber were defined according to [15].

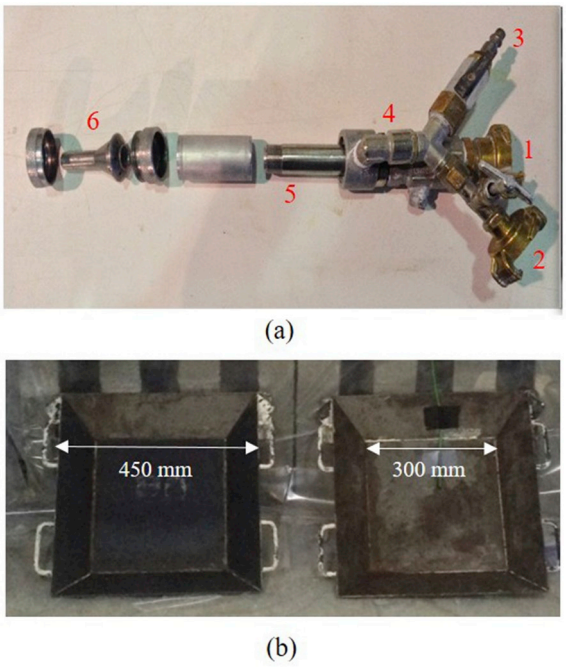

Fig. 4. (a) Spray gun and (b) dimensions of the metal panels.

2.5. Test methods

Table 4 presents the tests performed with sprayed pastes and mortars. Their descriptions are presented subsequently. The moment of accelerator addition was considered as the initial time (0 s) for all tests and results.

Powder XRD was performed with the ID and REF mixes. The objective of this test was to quantify the phases formed during hydration at early ages. Sprayed pastes were frozen in liquid nitrogen to stop hydration at 15 min, 1 h, 3 h and 12 h after accelerator addition. Then, they were crushed and ground to a maximum size of 63 μm. Pastes were not lyophilized because the stability and crystallinity of ettringite and monosulfoaluminate could be compromised, as indicated by Ref. [20].

A PANalytical X'Pert PRO MPD Alpha1 powder diffractometer in reflection Bragg-Brentano θ/2θ geometry using Ni-filtered CuKα_1 radiation (λ = 1.5406 Å) with an X'Celerator detector (active length of 2.122°) operating at 45 kV and 40 mA was used. X-ray diagrams were obtained from 4 to 80°2θ, using a step width of 0.017°2θ and 50 s per step, with a fixed divergence slit of 0.5°. Sample holders were spun at 2 rps. The diagrams obtained in the pastes were analyzed semi-quantitatively by Rietveld analysis using the software X'Pert High Score Plus from PANalytical. All structure models used for Rietveld refinement are shown in Table 5.

Isothermal calorimetry was conducted to analyze the kinetics of hydration of sprayed mortars. Tests were performed with approximately 15 g of mortar for 24 h at 20 °C using an I-cal 4000 isothermal calorimeter. The mortar was sprayed directly into the calorimeter cups and introduced in the equipment immediately after spraying.

SEM was performed in pastes at the ages of 15 min and 12 h after accelerator addition. This analysis was conducted in a JEOL JSM 7100F microscope at the voltage of 20 kV. Pastes were frozen in liquid nitrogen to stop hydration, dried in vacuum during 24 h and coated with carbon. Morphology of the phases was analyzed in fracture surfaces and their chemical composition was assessed by energy dispersive X-ray analysis.

Needle penetration test was used to determine the penetration resistance of sprayed mortars until 2 h after accelerator addition. The test consisted of five penetrations of a needle into the mortar with a constant velocity of 60 mm/min until the penetration of 25 mm was reached. The result of force is divided by the sectional area of the needle to obtain the penetration resistance. Initial and final setting times were determined when the penetration resistance reached 3.5 MPa and 27.6 MPa, respectively.

Table 4
Tests performed on sprayed pastes and mortars.

Objective	Test	Age	Matrix	Specimen	Reference
Chemical characterization	Powder XRD	15 min and 1, 3, 12 h	Sprayed paste	Frozen and ground paste	[6,10]
	Isothermal calorimetry	0–24 h	Sprayed mortar	Fresh mortar	[6]
	SEM	15 min and 12 h	Sprayed paste	Freeze-dried paste	[6,10]
Mechanical properties	Needle penetration test	From 15 to 120 min every 15 min	Sprayed mortar	Mortar panels	[16]
	Pin penetration test	4, 6, 12 h	Sprayed mortar	Mortar panels	[17]
	Compression test	1, 3, 7, 28, 98 days	Sprayed mortar	Extracted cores	[18]
	Water accessible porosity	7, 28, 98 days	Sprayed mortar	Extracted cores	[19]

Table 5
Phase structures used for Rietveld refinement.

Phase	Formula	Crystal System	PDF Codes	ICSD	Ref
Alite	Ca_3SiO_5	Monoclinic	01-070-8632	94742	[21]
Belite	Ca_2SiO_4	Monoclinic (β)	01-083-0460	79550	[22]
Calcium Aluminate	$Ca_3Al_2O_6$	Cubic	00-038-1429	1841	[23]
Ferrite	Ca_2AlFeO_5	Orthorhombic	01-071-0667	9197	[24]
Gypsum	$CaSO_4^{2-}\cdot H_2O$	Monoclinic	00-033-0311	151692	[25]
Calcite	$CaCO_3$	Rhombohedral	01-083-0577	79673	[26]
Portlandite	$Ca(OH)_2$	Rhombohedral	01-072-0156	15741	[27]
Ettringite	$Ca_6Al_2(SO_4)_3\cdot(OH)_{12}\cdot 26H_2O$	Hexagonal	00-041-1451	155395	[28]
Monosulfoaluminate	$Ca_4Al_2(SO_4)\cdot(OH)_{12}\cdot 6H_2O$	Rhombohedral	–	24461	[29]

Pin penetration test was employed to assess the indirect compressive strength of sprayed mortars from 4 to 12 h after accelerator addition. The device used was a Windsor® WP-2000 gun with a pin of 3 mm of diameter and 30 mm of length. Each measurement corresponded to the average of 3 penetrations at each age. The indirect compressive strength was calculated by a correlation table provided in Ref. [30].

Compressive strength was assessed in mortar cores measuring 25 mm in diameter and 50 mm in length. Cores were extracted from the sprayed panels 24 h after finishing spraying and cured in water until the day of the test. Six cores were tested at each age, using a universal test machine with a pressure application rate of 0.45 MPa/min.

Water accessible porosity was determined with spray mortars according to [19]. Cores were extracted and cured following the same procedure of compressive test until the age of the test (7, 28 and 98 days). Three specimens by age and mixture were immersed in water for three days and their saturated weight (W_s) was measured after that. Then specimens were dried at 60 °C during five days and their dry weight (W_d) was determined. Water accessible porosity was calculated with equation (4).

$$Water\ accessible\ porosity = \frac{W_s - W_d}{W_d} \quad (4)$$

3. Results and discussion

3.1. Chemical characterization

3.1.1. Powder X-Ray diffraction

Fig. 5 shows the evolution of the phase composition in sprayed pastes

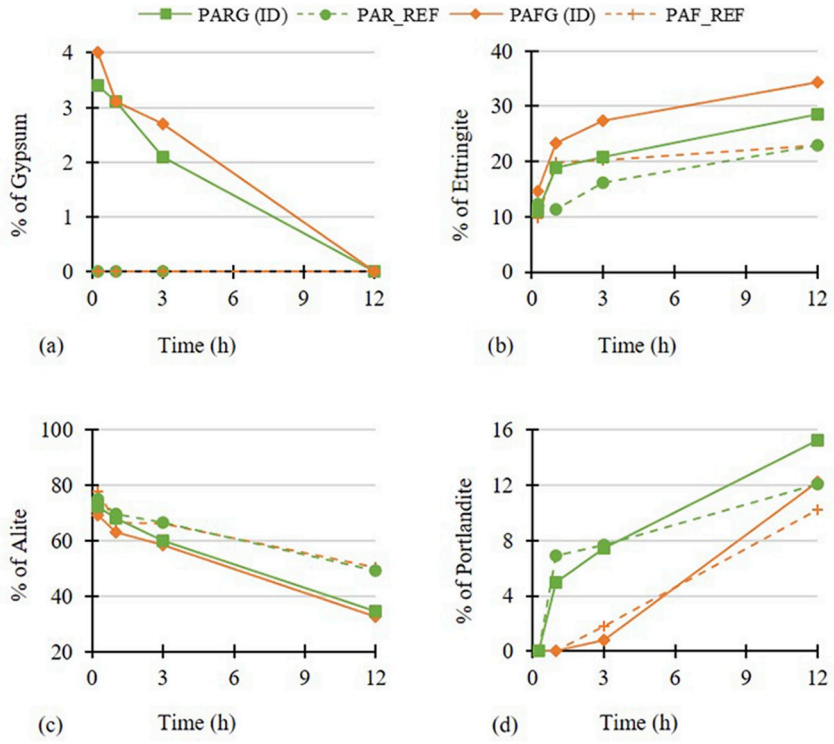

Fig. 5. Evolution of the content of the main phases found in sprayed paste: (a) Gypsum, (b) Ettringite, (c) Alite and (d) Portlandite.

during the first 12 h of hydration. To simplify the analysis, only gypsum (Fig. 5a), ettringite (Fig. 5b), alite (Fig. 5c) and portlandite (Fig. 5d) are presented. Slow reacting phases (belite and ferrite) were not included.

Fig. 5 a reveals that gypsum depletion in the reference paste occurs before the first measurement was done (15 min after accelerator addition). In mixes PARG (ID) and PAFG (ID), the same occurs between 3 and 12 h after accelerator addition. The earlier depletion of gypsum observed in REF mixes may limit the formation of ettringite by the reduction of sulfate concentration in the matrix.

Fig. 5 b confirms this hypothesis. The additional gypsum regulates the fast sulfate consumption caused by accelerators and promotes additional ettringite formation, similarly to the observed by Ref. [6]. At 1 h of hydration, ettringite amounts in pastes PARG (ID) and PAFG (ID) are 1.6 and 1.2 times larger than in the respective references. This initial effect is stronger in paste PARG (ID) due to the absence of sulfate in the formulation of the alkaline accelerator. Since ettringite is the main hydrate responsible for the early mechanical properties of sprayed matrices [31], a better performance is expected in ID mixes in comparison with the references.

Fig. 5 c reveals that alite hydration is also affected by the gypsum amount added to the system. In pastes PARG (ID) and PAFG (ID), with the additional gypsum, a proper sulfate balance is achieved. Therefore, accelerated undersulfated C_3A reactions and the consequent formation of AFm phases before the onset of alite hydration are mitigated. Thus, the precipitation of AFm phases on the surface of cement particles is limited [3]. As a result, alite hydration proceeds normally and higher degrees of hydration are reached at 12 h in comparison with the reference pastes.

Fig. 5 d shows that portlandite formation at 12 h of hydration in the ID mixes is from 1.26 to 1.21 higher than the REF mixes. Portlandite formation is enhanced due to the higher alite hydration in the ID mixes. In mixes PARG (ID) and PAR_REF, the formation is higher than in PAFG (ID) and PAF_REF. This difference occurs because the AR accelerator contains NaOH, which increases the concentration of OH^- ions in the liquid phase and promotes portlandite precipitation [32].

3.1.2. Isothermal calorimetry

Fig. 6 presents the heat of hydration curves of the 6 mixes. Fig. 6a and 6 b shows the heat of hydration from the accelerator peak that takes place in the period comprehended between 0 and 0.5 h. Fig. 6c and 6 d shows the heat flow until 24 h, highlighting the main hydration peak that takes place between 4 h and 10 h. Table 6 shows the characteristic points of the heat flow curves, calculated according to [6].

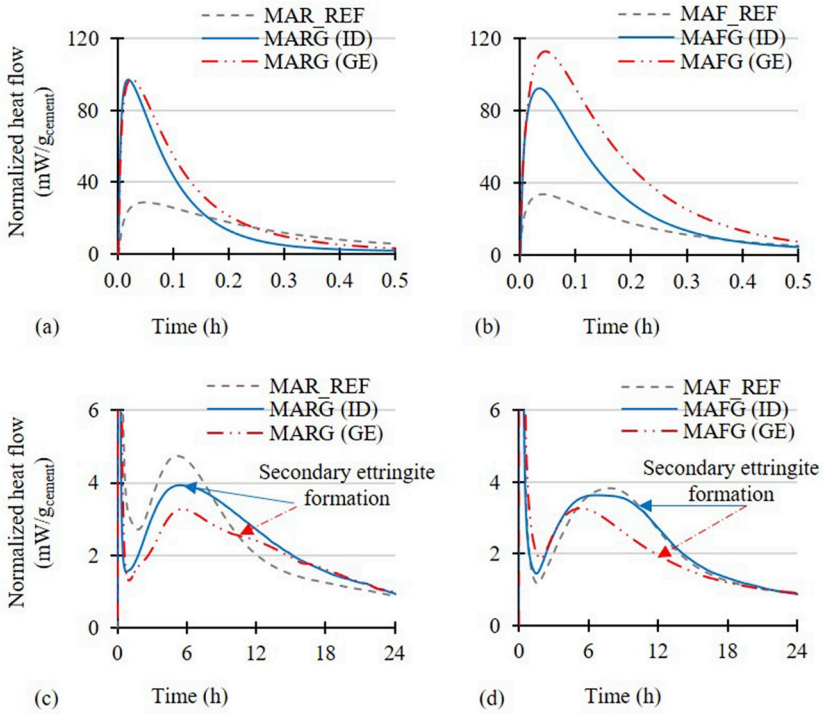

Fig. 6. Heat flow curves in cement mortars from 0 to 0.5 h with (a) alkaline and (b) alkali-free accelerator and from 0 to 24 h in cement mortars with (c) alkaline and (d) alkali-free accelerators.

Table 6
Characteristic points of the heat flow curves.

	Maximum heat-flow - accelerator peak (mW/g)	Slope - accelerator peak (mW/g*h)	Energy released - accelerator peak (J/g) [1]	Energy released - main peak (J/g) [2]	Maximum heat flow - main peak (mW/g)	Slope - main peak (mW/g*h)	Energy released until 24 h (J/g) [3]
MAR_REF	28.80	576.06	28.05	174.41	5.24	0.51	202.73
MARG (ID)	96.99	4974.66	39.91	197.30	4.02	0.51	204.11
MARG (GE)	97.34	3796.31	49.96	168.59	3.45	0.42	177.35
MAF_REF	33.71	693.60	27.33	160.77	3.83	0.47	186.87
MAFG (ID)	92.16	2632.03	54.96	171.07	3.63	0.42	192.40
MAFG (GE)	112.55	2206.56	67.36	138.73	3.27	0.39	171.88

[1] The energy released corresponds to the area under the heat flow curve from 0 to 0.5 h.
[2] The energy released corresponds to the area under the heat flow curve from the end of the induction period until the time when the heat flow reaches 1.1 mW/g of cement in the deceleration period.
[3] The energy released corresponds to the area under the heat flow curve until the 24 h minus the energy released in the accelerator peak.

The maximum heat flow, the energy released and the reaction rate during the accelerator peak depend on the amount of gypsum in the mortar, as observed in Fig. 6 and in Table 6. The values of these parameters are around three times higher in mortars ID and GE, when compared to the reference mixes. Likewise, mortars GE present a higher maximum heat flow and reaction rate than mortars ID.

The reason for this behaviour lies on the exothermic reaction of accelerators. Since ettringite precipitation is the main process that occurs due to accelerator reaction, gypsum additions favour the formation of this hydrate by increasing the sulfate concentration and, therefore, higher values of heat flow, reaction rate and energy released are observed. These results are in agreement with the XRD analysis (Fig. 5).

As shown in Fig. 6c and 6 d, the main hydration peak occurs several hours after the accelerator peak and is the result of alite and C_3A hydration. The first process forms portlandite and C—S—H, while the second generates ettringite. The shoulder caused by the reaction of the C_3A is indicated by the arrows in the curves from Fig. 6c and 6 d.

In reference mortars, the shoulder related with C_3A hydration overlaps with that generated by alite hydration, indicating that both processes occur simultaneously. Since reactions are exothermic, the maximum heat flow and the reaction rate in the main hydration peak are higher in reference samples.

A retardation on the reaction of the C_3A is observed when additional gypsum is used (mortars ID and GE). As the overlapping of the C_3A and alite hydration does not occur, the main hydration peak is wider in ID mortars. Moreover, the use of the ideal amount of gypsum increases the sulfate concentration and in consequence reduces the formation of AFm and favouring additional alite hydration. Therefore, mixes with the ideal gypsum content display the highest total energy released in the main peak. This increase in the degree of hydration may lead to higher mechanical strengths at this age in ID mixes.

The energy released during the main hydration peak in mortars GE is the lowest because the large gypsum amount used in this mortar inhibits alite dissolution by the common ion (Ca^{2+}) effect. Furthermore, as the aluminate and the silicate hydration compete to fill the spaces available in the matrix, the large amount of ettringite formed by accelerator reaction may reduce the space for the precipitation of the hydration products formed by alite hydration. Therefore, the more reactive accelerator reaction, limits the extent of alite dissolution and further hydration [33].

In the mixes with additional gypsum, the energy released in the accelerator peak of mortars produced with the alkali-free accelerators is always higher than the equivalent mortar produced with the alkaline accelerator. This occurs because the alkali-free accelerator contains dissolved sulfate ions in its composition. Therefore, accelerator reactivity is enhanced because it does not depend exclusively on the sulfates generated by gypsum dissolution, which occurs when the alkaline accelerator is used.

The accelerator type also influences the main hydration process. When the alkali-free accelerator is used, C_3A hydration is retarded when compared with the mixes produced with the alkaline accelerator. That is observed by the shoulder in the main hydration peak, which occurs at 8 and 9.5 h in mortars MARG (ID) and MAFG (ID), respectively. As a result, the maximum heat flow, the reaction rate and the energy released in the main hydration peak are reduced when the alkali-free accelerator is used.

The results of isothermal calorimetry indicate that the inclusion of additional gypsum may improve the reactivity of the mix. More energy was released during the accelerator peak, indicating the formation of larger amounts of ettringite, which may contribute to increasing the mechanical strength of the matrix after the accelerator reaction. Furthermore, alite reactivity is enhanced when the ideal dose of gypsum is used, which may improve the mechanical strength at late ages.

3.1.3. Scanning electron microscopy

Fig. 7 presents the SEM images of pastes PAR_REF and PARG (ID) at 15 min and 12 h. The regions analyzed by EDS are indicated by a circle in the corresponding image. EDS results are represented as relative intensities of each element, placed above each image. The peaks

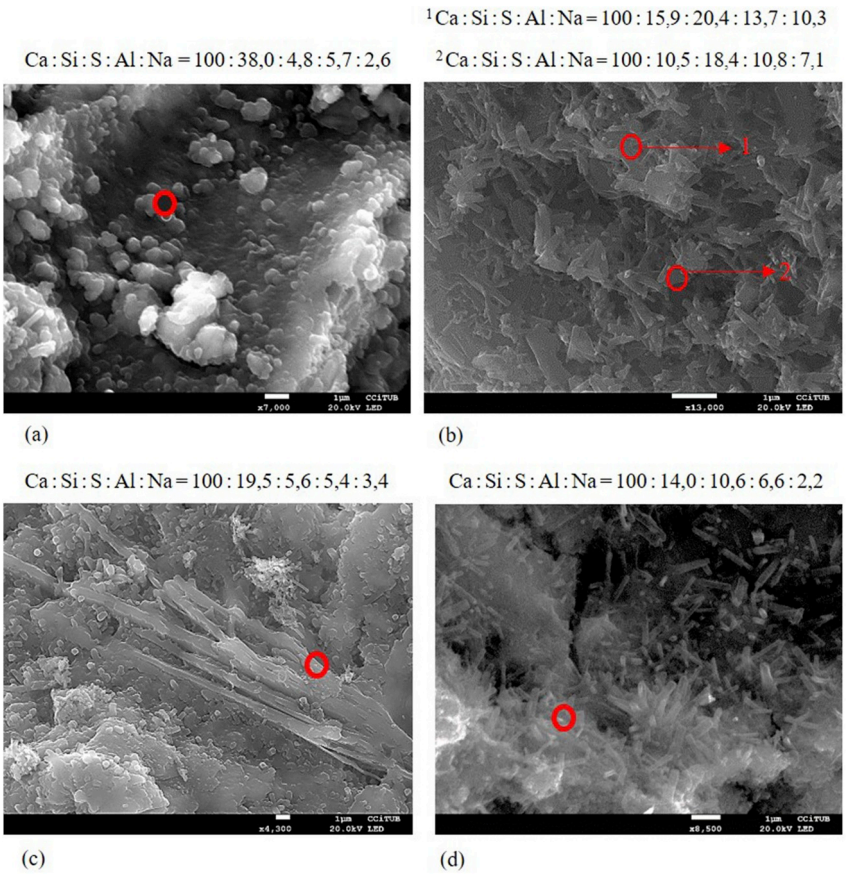

Fig. 7. Microstructure of (a) PAR_REF at 15 min, (b) PARG (ID) at 15 min, (c) PAR_REF at 12 h and (d) PARG (ID) at 12 h.

considered to measure the intensity of Ca, Si, Al, S and Na correspond to the energies of 3.7, 1.8, 1.5, 2.3 and 1.1 keV, respectively.

The microstructure observed in paste PAR_REF (Fig. 7a and 7 c) is heterogeneous. Hydrates formed by accelerator reaction at 15 min (Fig. 7a) are small plate-like precipitates. These hydrates are characterized by an Al/S ratio equal to 1.2, which indicates an early formation of AFm phases. This was also observed by Refs. [3,10] in cement pastes produced with alkaline accelerators.

However, when additional gypsum is employed, the microstructure of the matrix is significantly altered, as observed in Fig. 7 b. The hydrates formed are characterized by an Al/S ratio equal to 0.58–0.67, which indicates that ettringite is the main product formed by accelerator reaction and that gypsum remains in the matrix. The presence of AFm phases in paste PARG (ID) was not observed at 15 min and is in line with the results of XRD (Fig. 5) and isothermal calorimetry (Fig. 6), which indicate that accelerated undersulfated C_3A reactions are mitigated by an increase of sulfate concentration with the addition of gypsum.

At 12 h, the microstructure observed in paste PAR_REF (Fig. 7c) contained hydrates formed as plate-like crystals, which are embedded in the matrix. The Al/S ratio of the hydrates is equal to 0.98, which indicates they might be composed by AFm phases. The presence of AFm phases in paste PARG (ID) was not found at 12 h (Fig. 7d) and the microstructure of the aluminate hydrates continue to be needle-like crystals, with an Al/S ratio equal to 0.62. This suggests that ettringite is stable from 15 min to 12 h and that undersulfated C_3A reactions do not occur during this period.

Fig. 8 shows the microstructure of pastes PAF_REF and PAFG (ID) at 15 min and 12 h after the accelerator addition. In Fig. 8 a, the PAR_REF reveals a mix of AFt and AFm phases (Al/S = 0.98) at 15 min of hydration. On the other hand, the hydrates found in the mix PAFG (ID) at 15 min (Fig. 8b) were ettringite and gypsum (Al/S = 0.60–0.64). This tendency was maintained at 12 h, with Al/S ratios of 0.67 and 0.51 in the mixes PAF_REF and PAFG (ID), respectively. Except for the presence of sodium introduced by the alkaline-accelerator, these results are similar to those found for pastes with the alkaline accelerator.

3.2. Mechanical properties

3.2.1. Needle penetration test

Fig. 9 presents the average results of needle penetration resistance from 15 to 120 min after accelerator addition. It corresponds to the initial period of mechanical strength development.

The early development of mechanical strength depends on the additional gypsum incorporated. As analyzed in isothermal calorimetry (Table 6), the ettringite amount formed by accelerator reaction is directly proportional to the amount of gypsum added. Since ettringite is the main hydrate responsible for the initial evolution of mechanical strength [31], a higher penetration resistance is obtained by increasing the sulfate concentration when gypsum is added to the matrix.

A different trend was observed in the slope (rate of increase of penetration resistance) for both accelerator types. The slope of the estimated regression line is the highest in ID mixes, followed by REF and GE mixes. This means that the rate of increase of penetration resistance is higher when the ideal dose of gypsum is incorporated. This happens because accelerator reaction is enhanced with the increase of the sulfate concentration by the incorporation of gypsum.

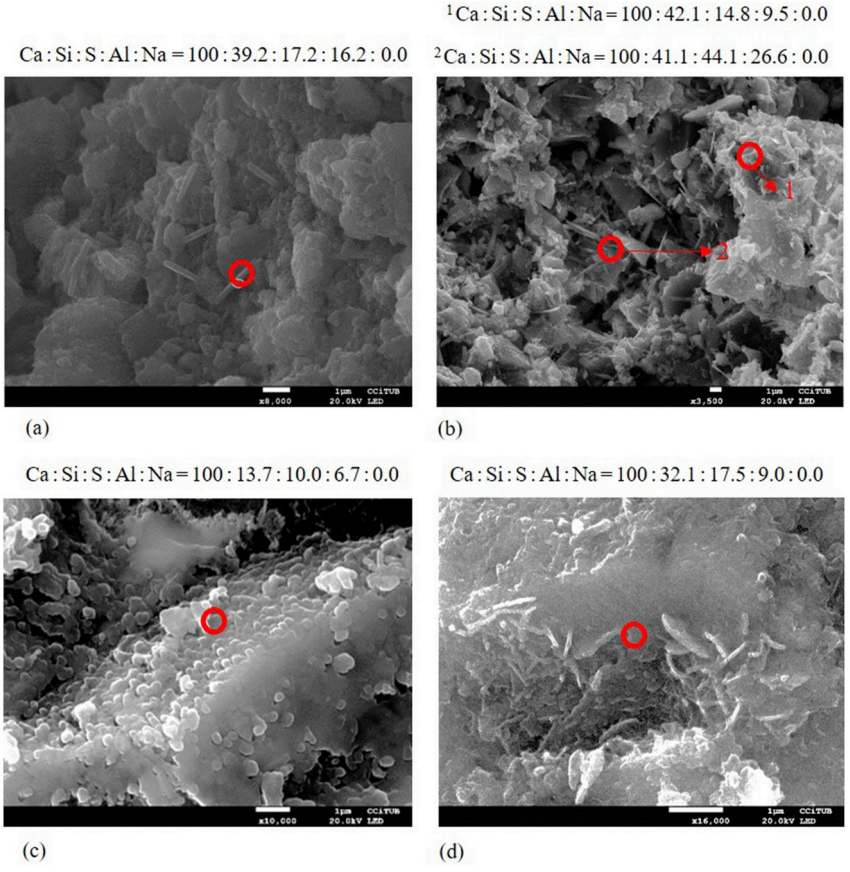

Fig. 8. Microstructure of (a) PAF_REF at 15 min, (b) PAFG (ID) at 15 min, (c) PAF_REF at 12 h and (d) PAFG (ID) at 12 h.

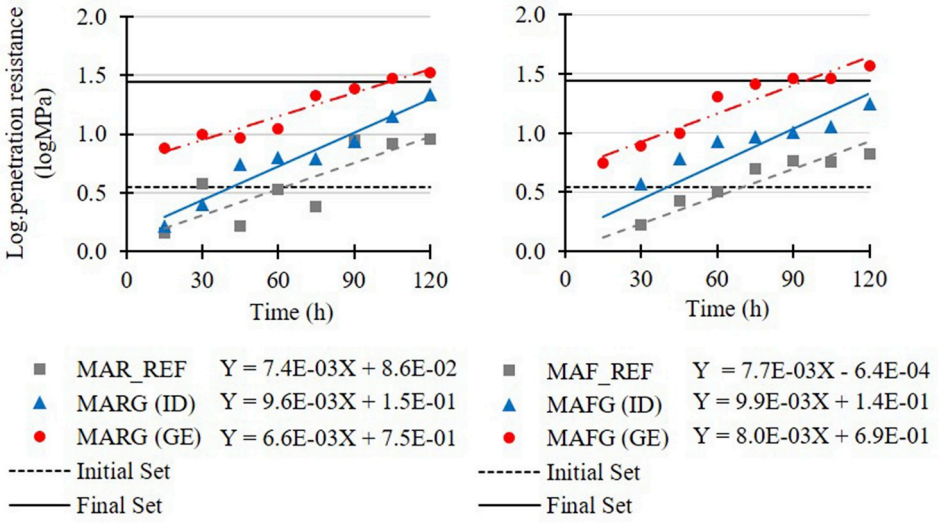

Fig. 9. Average results of needle penetration resistance in sprayed mortars with the (a) alkaline and (b) alkali-free accelerators.

The initial setting is reached before 15 min, at 40 min and after 60 min in GE, ID and REF mixes, respectively. An enhancement of accelerator reactivity reduces the time of the initial setting, according to the results of isothermal calorimetry. In line with that, the reference mixes require more time to set and harden.

The final setting follows the same pattern of the initial setting. It occurs at 1.5 h, 2.2 h and after 3 h in GE, ID and REF mixes, respectively. According to the isothermal calorimetry results (Fig. 6), GE mixes present the highest energy released during the accelerator peak, which is translated into a higher penetration resistance observed in these matrices.

3.2.2. Pin penetration test

Fig. 10 shows the average results of indirect compressive strength at 4, 6 and 12 h after the accelerator addition. This period corresponds to the main hydration peak in the curves of isothermal calorimetry (Fig. 6).

Results obtained in this test are significantly influenced by the amount of gypsum in the matrix. With both accelerator types, ID mixes presented the highest values of indirect compressive strength during the period analyzed. This happens because C_3A hydration is better controlled when the ideal amount of gypsum is used, increasing the sulfate concentration and in consequence avoiding a retardation in alite hydration by the early formation of AFm phases.

At 4h, mortars GE present a higher indirect compressive strength than reference mortars because the ettringite amount formed is larger due the enhanced accelerator reactivity caused by the sulfates in the gypsum addition. As hydration progresses, the opposite tendency is observed due to the possible excess of porosity caused by the fast setting of the GE mixes.

The mechanical strength from 4 to 12 h is directly proportional to the reaction rate observed in the main hydration peak obtained by isothermal calorimetry (Fig. 6). The ID mixes present the highest mechanical strength during the period analyzed due to the higher degree of alite hydration. At 12 h, the GE mixes present the lowest indirect compressive strength because alite dissolution and hydration are suppressed by the common ion effect (Ca^{2+} generated by gypsum dissolution) and by the large amount of ettringite formed by accelerator reaction, as discussed in the isothermal calorimetry results (Fig. 6).

3.2.3. Compressive strength

In order to provide additional information to analyze the results of

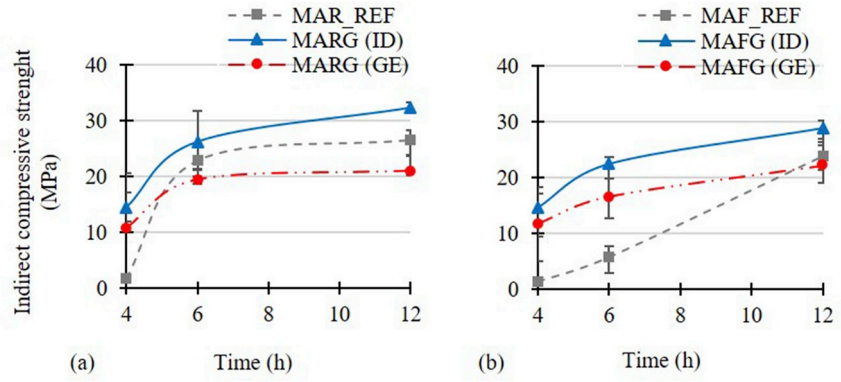

Fig. 10. Average results of indirect compressive strength obtained with (a) alkaline and (b) alkali-free accelerator.

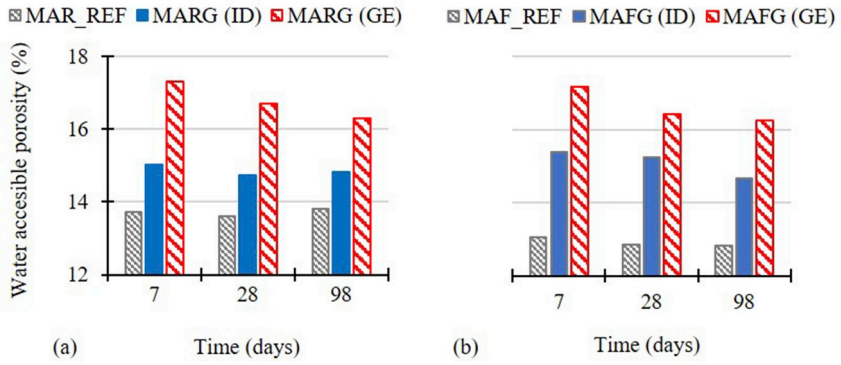

Fig. 11. Average results of water accessible porosity in sprayed mortars with (a) alkaline and (b) alkali-free accelerators.

compressive strength, the water accessible porosity results are shown in Fig. 11. An important difference is observed in the values of water accessible porosity when the concentration of sulfate is increased by the gypsum incorporation to the mortar. In all the cases, GE mixes present the highest porosity, while the REF mixes present the lowest. This follows the inverse order observed in the penetration resistance test (Fig. 9).

When large gypsum amounts are employed, ettringite formation is favoured by the increase of the sulfate concentration, reducing the setting time of the mortar. Due to the fast setting, mortars do not consolidate properly and do not eliminate entrapped air during the spraying process, which leads to higher porosities [9].

The reduction in the values of WAP from 7 to 98 days is the highest in GE mixes and the lowest in REF mixes. This happens because the additional gypsum increases the sulfate concentration and retards the conversion of ettringite to monosulfoaluminate [7], which occurs with increases in porosity because ettringite has lower density and higher molecular volume than monosulfoaluminate [9]. Since alite hydration is not inhibited by undersulfated C_3A reactions, pores are filled by portlandite and C—S—H, reducing the total porosity of the matrix.

Fig. 12 presents the average results of compressive strength obtained with extracted cores at 1, 3, 7, 28 and 98 days (time in logarithmic scale). Similarly, to the evaluation of water accessible porosity, compressive strength varies significantly in mortars with gypsum addition.

ID mixes present the highest compressive strength at all ages. As observed in XRD and isothermal calorimetry (Figs. 5 and 6), mixes with the ideal amount of gypsum present a higher degree of hydration because accelerated undersulfated C_3A reactions are avoided and alite hydration proceeds normally.

Despite being less porous, mortars REF present smaller compressive strength than mortars ID. In REF samples, AFm phases generated by undersulfated C_3A reactions precipitate on the surface of cement particles. This decreases their solubility and degrees of hydration, also reducing the compressive strength. The lowest values of compressive strength are found in GE mortars because they have the highest porosity (Fig. 11).

4. Conclusions

The following conclusions may be derived from the results obtained in this study.

- The increase of sulfate concentration by the addition of gypsum in sprayed mixes leads to a faster formation of ettringite by increasing the reactivity of alkali-free and alkaline accelerators. Since ettringite is the main hydrate responsible for the development of initial mechanical strength, an increase in the penetration resistance of mortar is achieved. The effect is more relevant in matrices produced with the alkaline accelerators because they do not contain sulfates in

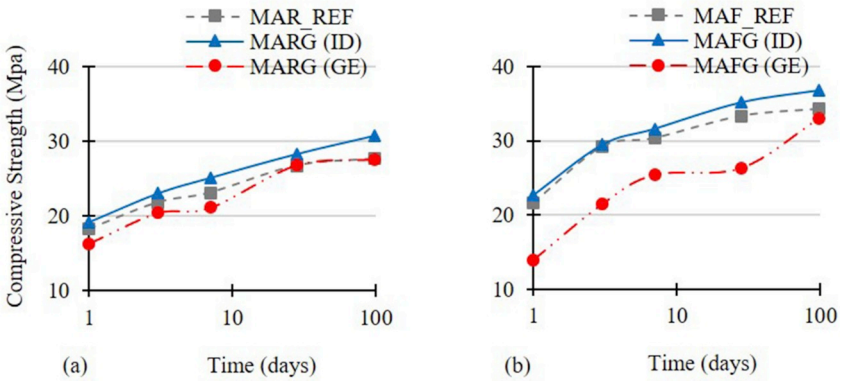

Fig. 12. Average results of compressive strength in sprayed mortars with (a) alkaline and (b) alkali-free accelerators.

their formulation.

- The use of a proper sulfate balance (ID mixes) in the matrix is a key factor to optimize the reactivity and the mechanical properties of sprayed mortars containing accelerators at short and long term. A significant improvement in performance may be achieved in mixes with accelerator by using cement specially designed for spraying or by incorporating gypsum as an addition. In the present study, the best performance was obtained for mixes with C_3A/SO_3 equal to 0.66, defined according to Eq. (1).
- The introduction of an excess of gypsum (GE mixes) suppresses alite dissolution due to the common ion (Ca^{2+}) effect. It also causes the formation of the largest amount of ettringite by accelerator reaction, which fills up the pores of the matrix before the onset of the main hydration peak and leads to more porous matrices. Therefore, the compressive strength of mortars GE is the lowest in the period analyzed.
- The benefits of using an optimum dose of gypsum were observed in mixes with alkali-free and alkaline accelerators. They were more evident in the latter due to the absence of sulfates in the formulation of alkaline accelerators. Therefore, the correction of the sulfate content by the gypsum addition in the mix is especially advisable in case of using this type of accelerator.

Acknowledgements

The first author would like to thank the CONICIT (Consejo Nacional para Investigaciones Científicas y Tecnológicas, process FI-108B-14) of Costa Rica for the scholarship granted. The second author would like to thank FAPESP (Fundação de Amparo à Pesquisa do Estado de São Paulo, process 2017/00125-9) for the scholarship granted. This research was possible due to the project RTC-2015-3185-4 (MAPMIT), cofunded by the Ministerio de Economía y Competitividad of Spain in the Call Retos-Colaboración 2015 and by the European Union through FEDER funds under the objective of promoting the technological development, innovation and high quality research. Thanks for technical and financial support are extended to Industrias Químicas del Ebro, to Centro para el Desarrollo Industrial (CDTi) and to the Ministerio de Economía y Competitividad, all of them in the context of the project IDI-20130248.

References

[1] I. Galobardes, S.H.P. Cavalaro, A. Aguado, T. Garcia, Estimation of the modulus of elasticity for sprayed concrete, Construct. Build. Mater. 53 (2014) 48–58, https://doi.org/10.1016/j.conbuildmat.2013.11.046.
[2] L.R. Prudêncio, Accelerating admixtures for shotcrete, Cement Concr. Compos. 20 (1998) 213–219, https://doi.org/10.1016/S0958-9465(98)80007-3.
[3] R.P. Salvador, S.H.P. Cavalaro, I. Segura, A.D. Figueiredo, J. Pérez, Early age hydration of cement pastes with alkaline and alkali-free accelerators for sprayed concrete, Construct. Build. Mater. 111 (2016) 386–398, https://doi.org/10.1016/j.conbuildmat.2016.02.101.
[4] I. Galobardes, R.P. Salvador, S.H.P. Cavalaro, A.D. Figueiredo, C.I. Goodier, Adaptation of the standard EN 196-1 for mortar with accelerator, Construct. Build. Mater. 127 (2016) 125–136, https://doi.org/10.1016/j.conbuildmat.2016.09.147.
[5] I. Galobardes, S.H.P. Cavalaro, C.I. Goodier, S. Austin, Á. Rueda, Maturity method to predict the evolution of the properties of sprayed concrete, Construct. Build. Mater. 79 (2015) 357–369, https://doi.org/10.1016/j.conbuildmat.2014.12.038.
[6] R.P. Salvador, S.H.P. Cavalaro, M. Cincotto, A.D. Figueiredo, Parameters controlling early age hydration of cement pastes containing accelerators for sprayed concrete, Cement Concr. Res. J. 89 (2016) 230–248 10.1016.
[7] A. Quennoz, K.L. Scrivener, Hydration of C3A–gypsum systems, Cement Concr. Res. 42 (2012) 1032–1041, https://doi.org/10.1016/j.cemconres.2012.04.005.
[8] A. Quennoz, K.L. Scrivener, Interactions between alite and C_3A-gypsum hydrations in model cements, Cement Concr. Res. 44 (2013) 46–54, https://doi.org/10.1016/j.cemconres.2012.10.018.
[9] R.P. Salvador, S.H.P. Cavalaro, R. Monte, A.D. Figueiredo, Relation between chemical processes and mechanical properties of sprayed cementitious matrices containing accelerators, Cement Concr. Compos. 79 (2017) 1–40, https://doi.org/10.1016/j.cemconcomp.2017.02.002.
[10] R.P. Salvador, S.H.P. Cavalaro, M. Cano, A.D. Figueiredo, Influence of spraying on the early hydration of accelerated cement pastes, Cement Concr. Res. 88 (2016) 7–19, https://doi.org/10.1016/j.cemconres.2016.06.005.
[11] I. Galobardes Reyes, Characterization and Control of Wet-mix Sprayed Concrete with Accelerators (Ph.D Thesis), Polytechnic University of Catalunya, 2013.
[12] AENOR, UNE-EN 1015-3, Methods of Test for Mortar Fon Mansory. Part 3: Determination of Consistency of Fresh Mortar, (2000) (by flow table).
[13] L. Agulló, T. Garcia, A. Aguado, Verificación de la isotropía del hormigón proyectado por vía húmeda, Mater. Construcción 59 (2009) 19–30.
[14] J. Woodward, An Introduction to Geotechnical Processes, First Edit, New York, 2005.
[15] AENOR, UNE-EN 14488-1 Ensayos de hormigón proyectado parte 1: toma de muestra de hormigón fresco y endurecido, (2006).
[16] ASTM C403/C 403M-08, Standard test method for time of setting of concrete mixtures by penetration resistance, Am. Soc. Test. Mater. i (2008) 1–7.
[17] AENOR, UNE EN 14488-2 ensayos de hormigón proyectado parte 2: resistencia a compresión del hormigón proyectado a corta edad, (2007).
[18] ASTM, ASTM, C39 standard test method for compressive strength of cylindrical concrete specimens 1, ASTM Int. i (2008) 1–7.
[19] AENOR, UNE 83890:2014. Concrete Durability. Test Methods. Determination of Water Absorption, Density and Accessible Porosity for Water in Concrete, (2014).
[20] J. Zhang, G.W. Scherer, Comparison of methods for arresting hydration of cement, Cement Concr. Res. 41 (2011) 1024–1036, https://doi.org/10.1016/j.cemconres.2011.06.003.
[21] M.A.G. de la Torre, A.G. Bruque, S. Campo, J. Aranda, The superstructure of C_3S from synchrotron and neutron powder diffraction and its role in quantitative phase analyses, Cement Concr. Res. 32 (2002) 1347–1356.
[22] M.D.T. Kamiya, Crystal structure and hydration of belite, Ceram. Trans. 40 (1994) 19–25.
[23] J.W. Mondal, P. Jeffery, The crystal structure of tricalcium aluminate, $Ca_3Al_2O_6$, Acta Crystallogr. B 31 (1975) 689–697.
[24] S. Colville, A.A. Geller, The crystal structure of brownmillerite, Ca_2FeAlO_5, Acta Crystallogr. B 27 (1971) 2311–2315.
[25] J.J. Chen, J.J. Thomas, H.F.W. Taylor, H.M. Jennings, Solubility and structure of calcium silicate hydrate, Cement Concr. Res. 34 (2004) 1499–1519, https://doi.org/10.1016/j.cemconres.2004.04.034.
[26] R. Wartchow, Learnt profile"-Methode(LP) fuer Calcit und Vergleich mit der “Background peak background”-Methode (BPB), Zeitschrift Fuer Krist. Krist. Krist. Krist. 186 (1989) 300–302.
[27] H.E. Petch, The hydrogen positions in portlandite, $Ca(OH)_2$, as indicated by the electron distribution, Acta Crystallogr. 14 (1961) 950–957.
[28] J. Goetz-Neunhoeffer, F. Neubauer, Refined ettringite ($Ca_6Al_2(SO_4)_3(OH)_{12}$*$26(H_2O)$) structure for quantitative X-ray diffraction analysis, Powder Diffr. (2006) 4–11.
[29] R. Allmann, Die Doppelschichtstruktur der plaettchenfoermigen Calcium-Aluminium-H Salze am Beispiel des $(CaO)_3Al_2O_3CaSO_4(H_2O)_{12}$, Neues Jahrb. Fuer Mineral. Monatshefte. (1968) 140–144.
[30] James Instruments, Windsor pin system WP-2000, Instruction manual (2010) 25.
[31] C. Maltese, C. Pistolesi, A. Bravo, T. Cerulli, D. Salvioni, M. Squinzi, Formation of nanocrystals of AFt phase during the reaction between alkali-free accelerators and hydrating cement: a key factor for sprayed concretes setting and hardening, RILEM Proc. PRO 45 (2005) 329–338.
[32] A. Kumar, G. Sant, C. Patapy, C. Gianocca, K.L. Scrivener, The influence of sodium and potassium hydroxide on alite hydration: experiments and simulations, Cement Concr. Res. 42 (2012) 1513–1523, https://doi.org/10.1016/j.cemconres.2012.07.003.
[33] P. Juilland, Early Hydration of Cementitious Systems, phD Thesis École Polytechnique Fédérale de Laussane, 2009.